



Cell-permeable bone morphogenetic protein 2 facilitates bone regeneration by promoting osteogenesis

Mingu Kang^{a,1}, Seokwon Lee^{a,1}, Jong-pil Seo^b, Eun-bee Lee^b, Daye Ahn^a, Jisoo Shin^a, Young-Ki Paik^{a,*}, Daewoong Jo^{a,**}

^a Cellivity R&D Institute, Cellivity Therapeutics, Inc., Seoul, 03929, South Korea

^b College of Veterinary Medicine and Veterinary Medical Research Institute, Jeju National University, Jeju, 63243, South Korea

ARTICLE INFO

Keywords:

Bone morphogenetic protein
Advanced macromolecule transduction domain
Cell permeability
Osteogenesis
Osteogenic agent
Biobetter

ABSTRACT

The use of the FDA-approved osteoinductive growth factor BMP2 is widespread for bone regeneration. However, its clinical application has been hindered by limitations in cell permeability and a short half-life in circulation. To address this issue, we have developed a modified version of BMP2, referred to as Cell Permeable (CP)-BMP2, which possesses improved cell permeability. CP-BMP2 incorporates an advanced macromolecular transduction domain (aMTD) to facilitate transfer across the plasma membrane, a solubilization domain, and recombinant human BMP2. Compared to traditional rhBMP2, CP-BMP2 exhibits enhanced cell permeability, solubility, and bioavailability, and activates Smad phosphorylation through binding to BMP receptor 2. The effectiveness of CP-BMP2 was evaluated in three animal studies focusing on bone regeneration. In the initial study, mice and rabbits with critical-size calvarial defects received subcutaneous (SC) injections of CP-BMP2 and rhBMP2 (7.5 mg/kg, 3 injections per week for 8 weeks). Following 8 weeks of administration, CP-BMP2 demonstrated a remarkable 65 % increase in bone formation in mice when compared to both the vehicle and rhBMP2. Moreover, rabbits exhibited faster bone formation, characterized by a filling pattern originating from the center. In a subsequent study involving injured horses, hind limb bones treated with CP-BMP2 exhibited an 85 % higher bone regeneration rate, as evidenced by Micro-CT results, in contrast to horses treated with the vehicle or rhBMP2 (administered at 150 µg/defect, subcutaneously, once a week for 8 weeks, without a scaffold). These results underscore the potential of CP-BMP2 to facilitate rapid and effective healing. No noticeable adverse effects, such as ectopic bone formation, were observed in any of the studies. Overall, our findings demonstrate that CP-BMP2 holds therapeutic potential as a novel and effective osteogenic agent.

1. Introduction

Bone repair is influenced by a variety of cellular, chemical and mechanical cues, which regulates the local regeneration and remodeling of bones in response to changes or failure in the healing process [1]. The interactive and interdependent bone-healing process requires a localized and sustained supply of essential factors such as osteogenic growth factors and cytokines. However, limited quantities or an imbalance of these factors is common in older people, particularly women, leading to delayed recovery from severe fracture. To overcome this, patients in such situations require long-term treatment with exogenous osteogenic factors [2].

The osteogenic factors used in clinical treatments include bone morphogenetic proteins (BMPs), fibroblast growth factor (FGF)-2, concentrated growth factors and vitamin D [3]. BMP2, a member of the transforming growth factor- β (TGF- β) superfamily, is the key player in bone formation. When BMP2 binds to cell-surface receptors, it triggers osteoblast differentiation and osteoinductive activity, playing a crucial role in bone formation during development, fracture healing, and spinal fusion [4–9]. BMP2 signaling is initiated through interactions between BMP2 and its transmembrane receptors, the BMPRs (type I and II serine/threonine kinase receptors), leading to the activation of (phosphorylation) Smads [10]. BMPR1-activated signaling results in the phosphorylation of R-Smads (Smad1/5/9), which bind to the common Smad, Smad 4, and regulate target gene transcription in the nucleus [11,

* Corresponding author. Cellivity Therapeutics, Inc., K-BIZ DMC Tower F9, 189 Sungam-Ro, Mapo-Gu, Seoul, 03929, South Korea.

** Corresponding author.

E-mail addresses: paiky@gmail.com (Y.-K. Paik), ceo@cellivity.com (D. Jo).

¹ These authors contributed equally to this work and share first authorship.

<https://doi.org/10.1016/j.mtbio.2024.100983>

Received 13 November 2023; Received in revised form 12 January 2024; Accepted 25 January 2024

Available online 1 February 2024

2590-0064/© 2024 The Authors. Published by Elsevier Ltd. This is an open access article under the CC BY-NC-ND license (<http://creativecommons.org/licenses/by-nc-nd/4.0/>).

Abbreviation

BMP	Bone morphogenic proteins
aMTD	Advanced macromolecular transduction domains
CPP	Cell-penetrating peptide
SD	Solubilization domain
IV	Intravenous
SC	Subcutaneous
CT	Computed tomography

[12]. Meanwhile, BMPR2-activated signaling promotes the expression of bone-related transcriptional regulators such as Runx2/Cbfa1, osterix, SIP1, Smurf1, NF- κ B, Hoxc-8 and Tob [13].

Numerous studies have demonstrated that recombinant human (rh) BMP2 can induce osteoblast differentiation through the mobilization of various mesenchymal cells or preosteoclasts such as C3H10T1/2 and MC3T3-E1 cells [14,15] or by redirecting C2C12 myoblasts to differentiate into osteoblasts and suppressing myogenic differentiation [11]. As the only FDA-approved osteoinductive growth factor that can be used as a bone graft substitute, rhBMP2 has been extensively studied for its potential applications in a wide range of biomedical fields, from orthopedic surgery to dental implantation [16]. The proprotein form of BMP2 contains 453 amino acid (aa), and the mature form comprises 114 aa residues that are subjected to posttranslational modification, dimerization and proteolytic cleavage by furin in the Golgi apparatus [17]. The biologically active form of rhBMP2 consists of monomers that form a covalent homodimer through a single disulfide bond between the Cys-78 residues in the two subunits [18–20].

Despite its osteogenic potential in bone tissue engineering and regenerative medicine, rhBMP2's clinical application as a protein-based therapeutic is limited by its weak biological activity. This is mainly due to its short half-life and instability in circulation [21,22]. Moreover, the poor retention of rhBMPs at implantation sites leads to rapid diffusion and clearance, reducing efficacy [23]. High doses are often required to sustain the osteogenic effect, but these doses can be costly and cause toxicity or unexpected ectopic bone formation [24]. To overcome these limitations, various delivery interfaces, such as scaffolds, grafts, and gels, are utilized to achieve the controlled release of rhBMP2 and its effective intracellular delivery [25,26]. This can be achieved by placing rhBMP2 inside a space-filling scaffold or releasing it directly from the surface of various carrier materials, including ceramics, metals, or synthetic polymers [22,27–31]. By using materials that facilitate local delivery and diffusion, rhBMP2 can be retained at the implantation site for prolonged period, promoting the regenerative process in the bone microenvironment [32].

A strategy to enhance the effectiveness of rhBMP2 therapy is the integration of a protein transduction domain (PTD), such as TAT (GRKKRRQRRRQ) peptide or similar forms [33,34]. However, the TAT peptide has a limited lifespan because it is taken into cells through endocytosis, leading to its degradation inside the cell and preventing the transfer of recombinant proteins from cell to cell. This transfer is crucial for the systemic delivery of exogenous macromolecules and tissue permeability [35].

To address the side effects and short half-life of rhBMP2, we used an optimized hydrophobic cell-penetrating peptide (CPP) called advanced macromolecule transduction domain (aMTD). aMTD increases tissue permeability and systemic delivery of exogenous proteins by penetrating the plasma membrane [36]. By combining rhBMP2 and a sequence-optimized aMTD (i.e., aMTD442), we created CP-BMP2, which is a new cell-permeable form of rhBMP2. We expect that CP-BMP2 will overcome the limitations of rhBMP2, such as weak treatment efficacy and instability in circulation, by improved cell permeability [36].

Here, we show that the novel recombinant protein CP-BMP2, which is derived from BMP2, has improved cell permeability, tissue delivery, and bone regeneration compared to rhBMP2. These findings suggest that CP-BMP2 has the potential to be a more effective therapeutic option for the treatment of bone defects.

2. Materials and methods

2.1. Construction of *E. coli* expression vectors for the recombinant BMP

The full-length cDNA for human BMP2 (RC214586) was purchased from Origene (Rockville, MD). To develop cell- and tissue-permeable recombinant BMP proteins, expression vectors were designed by fusing the DNA sequence of mature form (aa 282–396) encoding the *human BMP2* gene with an aMTD and/or solubilization domain (SD), and the aMTD sequence was not included in control BMP proteins (Fig. 1A and). Two different SDs were screened (SDA from protein S of *Myxococcus xanthus*, 184 aa; SDB from cytochrome *b* of *Rattus norvegicus*, 99 aa). Polymerase chain reaction (PCR) was carried out to generate the corresponding expression vectors for each recombinant BMP2 protein. The PCR mixture included 100 ng of genomic DNA, 10 pmol of each primer, 0.2 mM dNTP mixture, 1X reaction buffer and 2.5 U of Pfu(+) DNA polymerase (Doctor Protein, Korea), and the reaction included 40 cycles of denaturation (95 °C), annealing (58 °C), and extension (72 °C) for 30 s each, followed by a final extension cycle of 72 °C for 10 min. Then, the PCR products were cloned into a specific site of the pET-28a (+) vector (Novagen, Darmstadt, Germany), and DNA ligation was performed using T4 DNA ligase (NEB, USA) at 4 °C overnight. For transformation, the plasmids were mixed with *E. coli* BL21(DE3)-CodonPlus RIL competent cells (ATCC, USA) on ice for 10 min. This mixture was heat-shocked in a water bath at 42 °C for 90 s and then placed on ice for 2 min. Then, the mixture was added to LB broth (ELPIS, Korea) and incubated in a 37 °C shaking incubator for 1 h. The transformants were plated on an LB agar plate with kanamycin (50 μ g/mL). Plasmid DNA was extracted from a single colony, and after digestion with the restriction enzymes *Bam*HI and *Hind*III (NEB, USA), the sizes of the digested DNA fragments were confirmed by 1.2 % agarose gel electrophoresis.

2.2. Expression and purification of recombinant CP-BMP2 proteins

E. coli samples containing recombinant Recontide expression vectors (Fig. S1A) were incubated with 1 mL of LB medium at 37 °C overnight and then inoculated in 700 mL of LB medium, followed by incubation at 37 °C until the OD₆₀₀ reached ~0.7. Then, 0.7 mM isopropyl- β -D-thiogalactoside (IPTG), a protein expression inducer, was added to the culture medium, and the mixture was further incubated at 37 °C for 3 h. This culture medium was centrifuged at 4 °C and 8000 rpm for 15 min, and the supernatant was discarded to recover the cell pellet. The cell pellet was suspended in lysis buffer (50 mM NaH₂PO₄ and 300 mM NaCl, pH 8.0) and disrupted by sonication. The lysates were centrifuged at 15,000 rpm for 10 min to obtain an insoluble fraction containing recombinant protein. Denatured recombinant proteins were lysed using denaturing lysis buffer (8 M urea, 10 mM Tris, and 100 mM NaH₂PO₄) and purified using Ni-NTA resin. After washing the resin with denaturing wash buffer (8 M urea, 10 mM Tris, 20 mM imidazole, 100 mM NaH₂PO₄), recombinant BMP2 proteins were eluted 3 times with denaturing elution buffer (8 M urea, 10 mM Tris, 250 mM imidazole). After purification, the samples were dialyzed twice using refolding buffer (550 mM guanidine-HCl, 440 mM L-arginine, 50 mM Tris, 100 mM NDSB, 150 mM NaCl, 2 mM reduced glutathione and 0.2 mM oxidized glutathione). Finally, the buffer was replaced with a physiological buffer, such as DMEM, at 4 °C.

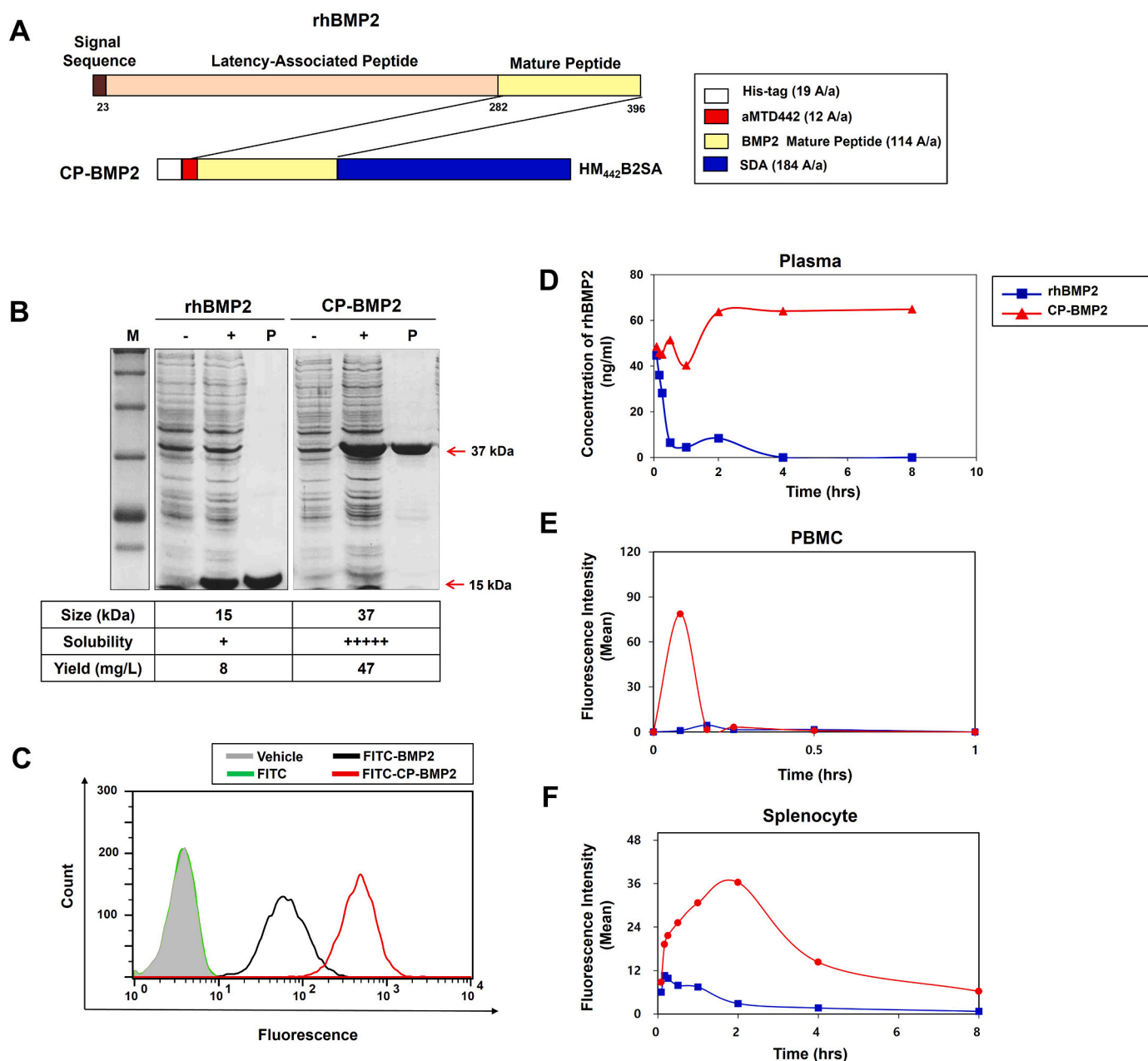


Fig. 1. Structure and physicochemical properties of CP-BMP2. (A) Schemes of the recombinant rhBMP2 and CP-BMP2 proteins and their components. (B) The expression, solubility and yield of rhBMP2 and CP-BMP2 proteins containing rhBMP2 and aMTD442. (C) Flow cytometry to detect the cell permeability of FITC-CP-BMP2 (red) in C2C12 cells. (D) CP-BMP2 levels in plasma over time. (E and F) Flow cytometry of FITC-labeled CP-BMP2 in peripheral blood mononuclear cells (PBMCs) (E) and splenocytes (F) over time. (For interpretation of the references to color in this figure legend, the reader is referred to the Web version of this article.)

2.3. Cell permeability analysis

For quantitative studies of cell permeability, CP-BMP2 (2 M – 3 and 2 M – 4) and control proteins without the aMTD and/or SD (2 M – 1, 2 M – 2, 2 M – 3C and 2 M – 4C) were conjugated to fluorescein isothiocyanate isomer (FITC) according to the manufacturer's instructions (Sigma–Aldrich). RAW 264.7 cells were treated with 10 μ M FITC-labeled recombinant proteins for 1 h at 37 °C in a 5 % CO₂ incubator and washed three times with 1X phosphate-buffered saline (PBS; HyClone™, GE Healthcare). Then, the cells were treated with 10 μ g/mL proteinase K (Sigma–Aldrich) for 20 min at 37 °C in a 5 % CO₂ incubator to remove proteins bound to the cell surface. The cell permeability of CP-BMP2 proteins was analyzed with a Guava® easyCyte™ benchtop flow cytometer (Millipore) by examining the median fluorescence intensity

(MFI) normalized to that of FITC-treated cells to obtain the relative cell permeability (fold change). To visualize the intracellular localization of CP-BMP2, NIH3T3 cells were treated with 10 μ M FITC-labeled proteins diluted in serum-free medium for 3 h at 37 °C in a 5 % CO₂ incubator and fixed with 4 % formaldehyde (Sigma–Aldrich) for 10 min at room temperature after washing with PBS. Intracellular delivery of these recombinant proteins was analyzed by confocal laser scanning microscopy (LSM700, Zeiss, Germany).

2.4. Ex vivo bioavailability test

Whole blood was obtained from ICR mice (male, 6 weeks) and mixed with Recontide and BMP2 lacking an aMTD. The ratio of protein to blood was 7.5 μ g protein per 1 mL blood based on the results of an *in vivo*

study. The blood and protein samples were allowed to react for different time periods (5, 10, 15, 30, 60, 120, 240, and 480 min). After the reaction, plasma was separated from the blood, and histidine in the plasma was detected by His-ELISA (GenScript).

2.5. *In vivo* bioavailability test

ICR mice (male, 6 weeks) were intravenously administered 30 mg/kg FITC-labeled CP-BMP2 or control rhBMP2. Then, the blood and spleen were collected 5 min to 36 h later. The blood was immediately placed in an EDTA tube and mixed well, followed by centrifugation at 4000 rpm and 4 °C for 5 min. Plasma was removed from the centrifuged blood, and the buffy coat was collected in a new microtube. Then, 0.5 mL of RBC lysis buffer was placed in the microtube, followed by vortexing. The microtube was left at room temperature for 5 min, followed by centrifugation at 4000 rpm and 4 °C for 5 min. When RBCs were not completely removed, 0.5 mL of RBC lysis buffer was added again, followed by vortexing. After removing the supernatant, the remaining pellet comprised peripheral blood mononuclear cells (PBMCs), and 0.3 mL of PBS was added, followed by pipetting. The spleen was separated into single cells in PBS using a slide glass or cell strainer. The cells were collected in a microtube, which was centrifuged at 4000 rpm and 4 °C for 5 min. After removing the supernatant, 0.5 mL of RBC lysis buffer was added, followed by vortexing. The microtube was incubated at room temperature for 5 min, followed by centrifugation at 4000 rpm and 4 °C for 5 min. When RBCs were not completely removed, 0.5 mL of RBC lysis buffer was added again, followed by vortexing. After removing the supernatant, the pellet containing splenocytes was resuspended in 0.5 mL of PBS by pipetting. PBMCs and splenocytes were subjected to fluorescence-activated cell sorting (FACS) analysis (FACSCalibur; BD, Franklin Lakes, NJ).

2.6. Western blot analysis to detect phosphorylated forms of Smad 1/5/9

The levels of p-Smad 1/5/9 were analyzed via western blot assay to demonstrate whether CP-BMP2 increases p-Smad 1/5/9 levels in C2C12 murine myoblast cells. After starvation with serum-free medium for 2 h, C2C12 cells (2×10^5 cells per well in 6-well plates) were treated with CP-BMP2 or BMP protein for 2 h at 37 °C. DPBS-washed cells were harvested with RIPA buffer (150 mM NaCl, 1 % Triton X-100, 0.1 % SDS, 2 mM EDTA and 50 mM Tris, pH 8.0) containing a protease and phosphatase inhibitor cocktail (Sigma). The quantified cell lysates were separated by 10 % SDS-PAGE, and the proteins were transferred to nitrocellulose membranes. The antibodies used were as follows: rabbit anti-phosphorylated Smad 1/5/9 (Cell Signaling, #13820), rabbit anti-Smad 1 (Cell Signaling, #6944S), and rabbit anti- β -actin (Cell Signaling, #4967).

2.7. Assessment of myotube formation

C2C12 murine myoblast cells were plated in 24-well culture plates (1×10^5 cells/well) in growth medium for 24 h. To induce differentiation, the cells were exposed to starvation conditions by incubation in culture medium containing 2 % FBS with or without CP-BMP2. After 3 days and 7 days of culture, the cells were photographed to evaluate differentiation into myotubes.

2.8. Measurement of alkaline phosphatase (ALP) activity

To investigate if CP-BMP2 directly affects osteogenic activity, C3H10T1/2 mesenchymal stem cells (1×10^5 cells per well in 24-well plates) were treated with BMP2 for 3 days or 7 days. ALP activity was measured in the cell lysates according to the manufacturer's protocol (cat # AS-72146). Briefly, the supernatant of the cell lysate was analyzed after centrifugation at 13,000 rpm for 10 min, and 10 μ l of this supernatant was reacted with 200 μ l of ALP substrate solution for 30 min at

37 °C. After 30 min, the optical density (OD) was measured by using a microplate reader at a wavelength of 405 nm. Different concentrations of *p*-nitrophenyl phosphate were used as standards for ALP activity, and the calculated ALP activity was normalized to the total protein concentration, which was obtained from the Bradford (Bio-Rad) protein assay.

2.9. Small interfering RNA-mediated silencing

For RNA interference, MC3T3-E1 preosteoblasts (2×10^5 cells per well in 6-well plates) were transfected with 10 or 15 nM siRNA (Dharmacon™ BMPR-II siGenome™ Smartpool, siBMPRII) in Opti-MEM. The cells were incubated for 4 h at 37 °C, and the medium was replaced with EGM-2 after 24 h. For treatments, cells were serum-starved in DMEM for 16 h and treated with CP-BMP2. Specific reductions in target protein levels were confirmed by western blot analysis wherever possible.

2.10. Mouse critical-sized calvarial defect model

The effect of CP-BMP2 on bone regeneration *in vivo* was investigated in a critical-sized calvarial defect model using ICR mice (6 weeks of age) (Dooyeol Biotech, Seoul, Korea). The mice were anesthetized with Zoletil (60 mg/kg) and xylazine (20 mg/kg), and the incision area was exposed by shaving the fur from the scalp. To create the defects, an incision was made in the skin on the head; two defects on both sides of the calvaria were made by using a 4-mm-diameter surgical trephine bur. The surgery sites were sutured and treated with povidone iodine. At 24 h after surgery, CP-BMP2 was locally injected into the surgery site, and the injection was repeated three times per week or once per week during the 8-week experimental period. All mice were sacrificed after 9 weeks, the calvarial bone was separated, and bone regeneration was examined by X-ray and micro-CT. The fixed calvarial tissues were exposed to soft X-rays (CMP-2, Softex Co., Tokyo, Japan) under optimized exposure conditions (23 kV, 2 mA, 90 s), and the films were developed. Three-dimensional micro-CT images were analyzed with Adobe Photoshop CS6 (Adobe Systems, CA, USA) to measure the regenerated bone areas.

2.11. Rabbit critical-sized calvarial defect model

Adult, skeletally mature male New Zealand white rabbits weighing 3.5–4 kg were randomly divided into 3 groups. Unilateral 15-mm-diameter critical-size defects were created in the calvarial bones of each animal. Group 1 served as a control group with unfilled calvarial defects. Group 2 had calvarial defects filled with rh-BMP2, and group 3 had calvarial defects filled with Recontide. All animals were killed 6 weeks after the initial surgery. The entire cranial vault was carefully removed from each animal with an oscillating saw, maintaining an intact galea, periosteum, and dura. The specimens were subjected to gross examination for signs of inflammation, photographed, fixed in 10 % buffered formalin, and subjected to micro-CT imaging before decalcification for histologic processing. The micro-CT results showed that group 1 had voids without bony bridges, group 2 had new bone regeneration on the peripheral side of the defect, and group 3 had island-like bony particles throughout the defect.

2.12. Surgical procedure: equine bone defect model (scaffold)

Horses were premedicated with 0.05 mg/kg medetomidine hydrochloride IV (Equadin, Dongbang Inc., Suwonsi, Korea). Five min later, 0.03 mg/kg diazepam (Diazepam Myi Amp., Myungin Pharm Co., Seoul, Korea) and 2.2 mg/kg ketamine (Yuhan Ketamine 50 Inj., Yuhan Pharm Co., Seoul, Korea) were administered IV. Thereafter, the horses were intubated through the trachea, placed on a surgical table in dorsal recumbency and subsequently anesthetized by the inhalation of isoflurane (Ifran, Hana Pharm Co., Seoul, Korea) in oxygen. Three skin incisions were made in each hindlimb, exposing the third metatarsal bone. The

first incision was made 8 cm distal to the proximal aspect of the third metatarsal bone, the second incision was made 3 cm distal to the first incision, and the third incision was made 3 cm distal to the second incision. At each of these incisions, a bone defect was drilled (Cordless Driver 4, Stryker, Seoul, Korea). The drill was inserted in the dorso-palmar direction. The diameter of the drilled holes was 5 mm, and the depth was 10 mm, as measured by a depth gauge. For the test without a scaffold and with weekly injections, the three treatments included control (saline), CP-BMP2, and BMP2 (2M1), and these treatments were applied to the three different holes in a randomized manner. The skin was sutured with absorbable sutures (2-0 Vicryl; Johnson and Johnson, Seoul, Korea) by a subcuticular method. After surgery, the three treatments were injected into each hole at 1-week intervals for 9 weeks. For the test with scaffold (collagen tape) implantation, the three treatments included control (saline) with scaffold, Recontide with scaffold, and BMP2 (2M1) with scaffold, and these treatments were inserted into the three holes in a randomized manner. The skin was sutured with absorbable sutures (2-0 Vicryl; Johnson and Johnson, Seoul, Korea) by a subcuticular method.

2.13. Postoperative treatment

After surgery, 1.1 mg/kg flunixin meglumine (Fluximine®, Bayer, Auckland, New Zealand) was administered IV twice daily for 3 days. Wound dressings were applied until 9 weeks after surgery and changed once weekly. Operative fields were washed with sterilized saline. Periodic postoperative clinical checks included evaluations of body temperature, heart rate, respiration rate, temperature around the surgical site, gastrointestinal motility, capillary refilling time, blood tests (complete blood counts and serum electrolyte levels), and pulse quality of the palmar digital artery. These examinations were conducted every day for the first 2 weeks and once weekly thereafter. Lameness was examined every week with a walk and trot test on a hard surface. All evaluations throughout the 9-week study period were conducted by the same veterinarian, who was blinded to the treatments.

2.14. Radiographic analysis

Radiography was conducted before the operation (pre), immediately following the operation, and at 1 week, 3 weeks, 5 weeks, 7 weeks and 9 weeks after the operation to evaluate healing at the bone defect sites (70 k International Co., Gyeonggi-do, Korea). Radiographic data were developed using an image reading system (Blade BMD, Medien International Co., Gyeonggi-do V, 0.08 s; lateromedial view for the second metatarsal bone with digital Radiography; Galaxy R, Medien, Korea).

2.15. Computed tomography evaluation

All horses were anesthetized with 2.2 mg/kg ketamine (Yuhan Ketamine 50 Inj., Yuhan, Seoul, Korea) and euthanized with 0.1 mL/kg T-61 (T-61, Hansoo Pharm Co., Gyeonggi-do, Korea) at 9 weeks after surgery. The legs were dissected from the body and examined using computed tomography (CT). The CT instrument (Somatom Emotion16, Siemens Ltd., Seoul, Korea) was calibrated using an air and water phantom before the test, and control areas were evaluated. Limbs were placed on the CT bed and examined. CT data were processed using three-dimensional image processing software (Syngo CT, Siemens Ltd., Seoul, Korea). Each image was resliced into three 0.5-mm-wide pieces using analytical software.

2.16. Statistical analyses

Statistical analyses were performed with GraphPad Prism software using an unpaired Student's *t*-test (two-tailed) when two groups were compared or using one-way ANOVA followed by Tukey's multiple comparisons test when more than two groups were compared.

Differences at $p < 0.05$ were considered statistically significant. Data are presented as the mean \pm SD or the mean \pm SEM.

3. Results

3.1. Screening of the structure optimized CP-BMP2 for intracellular delivery of rhBMP2

One of the major challenges in the clinical use of rhBMP2 is its short half-life in cells, plasma and tissues, which is largely determined by several intrinsic factors such as protein transfer, solubility, stability and cell localization. These factors are interrelated, making it difficult to find a straightforward solution to extend the half-life of rhBMP2. To improve its intracellular delivery of rhBMP2 to bone defect sites, we attempted to create a cell-permeable form of rhBMP2 by conjugating a sequence optimized peptide fragment known as aMTD to the N-terminal of the rhBMP2 mature peptide. aMTD is known to function as a driver engine [36], which can freely transfer proteins through membranes without energy, as demonstrated by Chung et al. [35]. To enhance the solubility of the conjugated rhBMP2, we also added a solubilization domain A (SDA) from the protein S of *Myxococcus xanthus* as described by Kobayashi et al. [37]. The resulting CP-BMP2 derivatives, are both cell-permeable and highly soluble bio-better drug candidates.

To find the best construct, 14 CP-BMP2 derivatives with a distinct aMTD sequences were created (Fig. S1A) and evaluated for their physicochemical properties, including solubility, yield, and cell permeability. Most of the CP-BMP2 derivatives showed improved solubility and yield (Fig. S1B). To assess cellular uptake, the fluorescein-5-isothiocyanate (FITC)-labeled proteins were incubated with C2C12 cells, a myoblast subclone. Some of CP-BMP2 derivatives exhibited much higher cell permeability than rhBMP2 without an aMTD (e.g., ca 11.5-fold higher for aMTD442 and 8.5-fold higher for aMTD24) (Fig. S1C). The best 4 CP-BMP2 derivatives were chosen based on solubility, yield and cell permeability. Their activity was then determined by evaluating relative alkaline phosphatase (ALP) activity as a marker for bone formation (Fig. S1D). Thus, aMTD442 was selected as the key driver sequence to be linked to CP-BMP2 for its superior cell permeability and ALP activity. Finally, we obtained the structurally optimized CP-BMP2, which is a 329 aa residue linear polypeptide with a weight of 37 kDa, consisting of a His-tag, aMTD442, mature rhBMP2 peptide, and SDA (184 aa) (Fig. 1A).

3.2. CP-BMP2 exhibits both improved cell permeability and stability

Having established CP-BMP2 as a lead candidate for bone regeneration study (Fig. 1A), we wanted to verify its molecular properties of CP-BMP2 in vitro and in vivo. First, we transfected into C2C12 cells with the expression vector (plasmid) encoding the CP-BMP2 gene and purified the resulting protein. The purified CP-BMP2 protein showed the expected molecular weight of 37 kDa and had good solubility and yield (Fig. 1B). It also had increased cell permeability in C2C12 cells as seen by flow cytometry (Fig. 1C). Next, we tested the stability of CP-BMP2 in vitro by administering it intravenously (IV) to mice and measuring the amount of BMP2 in plasma (>65 ng/mL) over 8 h, while that of rhBMP2 rapidly decreased within 30 min (Fig. 1D). This suggests that CP-BMP2a has a longer half-life than rhBMP2. To further examine the impact of the aMTD442 on the stability and uptake of CP-BMP2, we administered (IV) FITC-labeled rhBMP2 and CP-BMP2 protein to mice and evaluated their relative stability in cells. Our results showed that CP-BMP2 had a higher FITC intensity in peripheral blood mononuclear cells (PBMCs) and splenocytes compared to rhBMP2 (red-line in Fig. 1E and F). However, in the case of rhBMP2, there were essentially no noticeable peak signals within the same period of time measured (blue-line in Fig. 1E and F). These results suggest that CP-BMP2 is structurally stable with a longer half-life than rhBMP2 alone. We also investigated whether addition of aMTDs to rhBMP2 stimulates cellular uptake of CP-BMP2 in cells, found

that consistent with the results in plasma and splenocytes (Fig. 1D and E), the FITC intensity in cells treated with CP-BMP2 was much higher than that in cells treated with rhBMP2 (Fig. S2A). Additionally, CP-BMP2 remained in the blood and mice for a longer period of time than rhBMP2 (Fig. S2B and C). Overall, these results suggest that the addition of aMTD to rhBMP2 significantly improves the solubility, stability, cell permeability, and pharmacodynamics of rhBMP2, making CP-BMP2 a promising candidate for further study and potential clinical applications.

3.3. CP-BMP2 activates the BMP2 signaling pathway through BMPR2 binding

It is well known that a typical BMP2 signaling in canonical pathway confers Smad phosphorylation through binding to BMPR1 or BMPR2 [10]. To investigate if CP-BMP2 retains the biological activity of BMP2, we measured Smad phosphorylation in C2C12 cells by Western blot analysis. CP-BMP2 induced Smad phosphorylation (Fig. 2A–C) in a dose- and time-dependent manner similar to rhBMP2 (Fig. 2B and C). We confirmed that CP-BMP2 works through the BMPR2-mediated signaling pathway by treating transfected C2C12 cells with dorsomorphin (10 μ M), a BMPR inhibitor, and observing that it effectively blocked Smad phosphorylation induced by both CP-BMP2 and rhBMP2 (Fig. 2D). The depletion of rhBMPRII by its own siRNA reduced Smad phosphorylation by CP-BMP2 in treatment in C2C12 cells (Fig. 2E), further suggesting that CP-BMP2 triggers Smad phosphorylation via binding to BMPR2. BMPR is expressed in intracellular golgi apparatus or endoplasmic

reticulum (ER) [38]. Therefore, in order to prove that CP-BMP2 binds not only to BMPR on the membrane surface but also to BMPR in intracellular Golgi apparatus or ER, distribution location of CP-BMP2 in cells was analyzed using immunocytochemistry, and it was found that CP-BMP2 Localized to BMPR of Golgi or ER (Fig. 2F).

CP-BMP2 also blocked myotube formation in C2C12 cells (Fig. 2G) and increased ALP activity to a greater extent compared to rhBMP2 proteins (Fig. 2H), indicating that BMP2 in CP-BMP2 retains its biological activity.

3.4. CP-BMP2 promotes bone regeneration in a mouse critical-size calvarial defect model

To investigate if CP-BMP2 promotes bone regeneration through inducing osteogenesis in a clinical setting, we used a mouse model with critical-size calvarial defects, a commonly used method for analyzing bone regeneration analyses [39,40]. To determine the optimal drug dosage, we subcutaneously (SC) injected different doses (0.75, 3.75, 7.5, 15, 75, and 150 mg/kg) of CP-BMP2 into the mice once a week for a maximum of 8 weeks and found that the defects recovered in a dose-dependent manner when CP-BMP2 was used at the relatively lower doses (0.75–7.5 mg/kg). However, an increase in bone regeneration was not seen at a dose of 7.5 mg/kg or higher (Fig. 3A and B). After repeated SC injections of vehicle, rhBMP2 or CP-BMP2 at a dose of 7.5 mg/kg (3 times per week for 8 weeks), all mice were sacrificed, and bone regeneration was assessed using soft X-ray radiography and micro-CT imaging (Fig. 3C). The relative impact (*-fold change*) on bone regeneration was

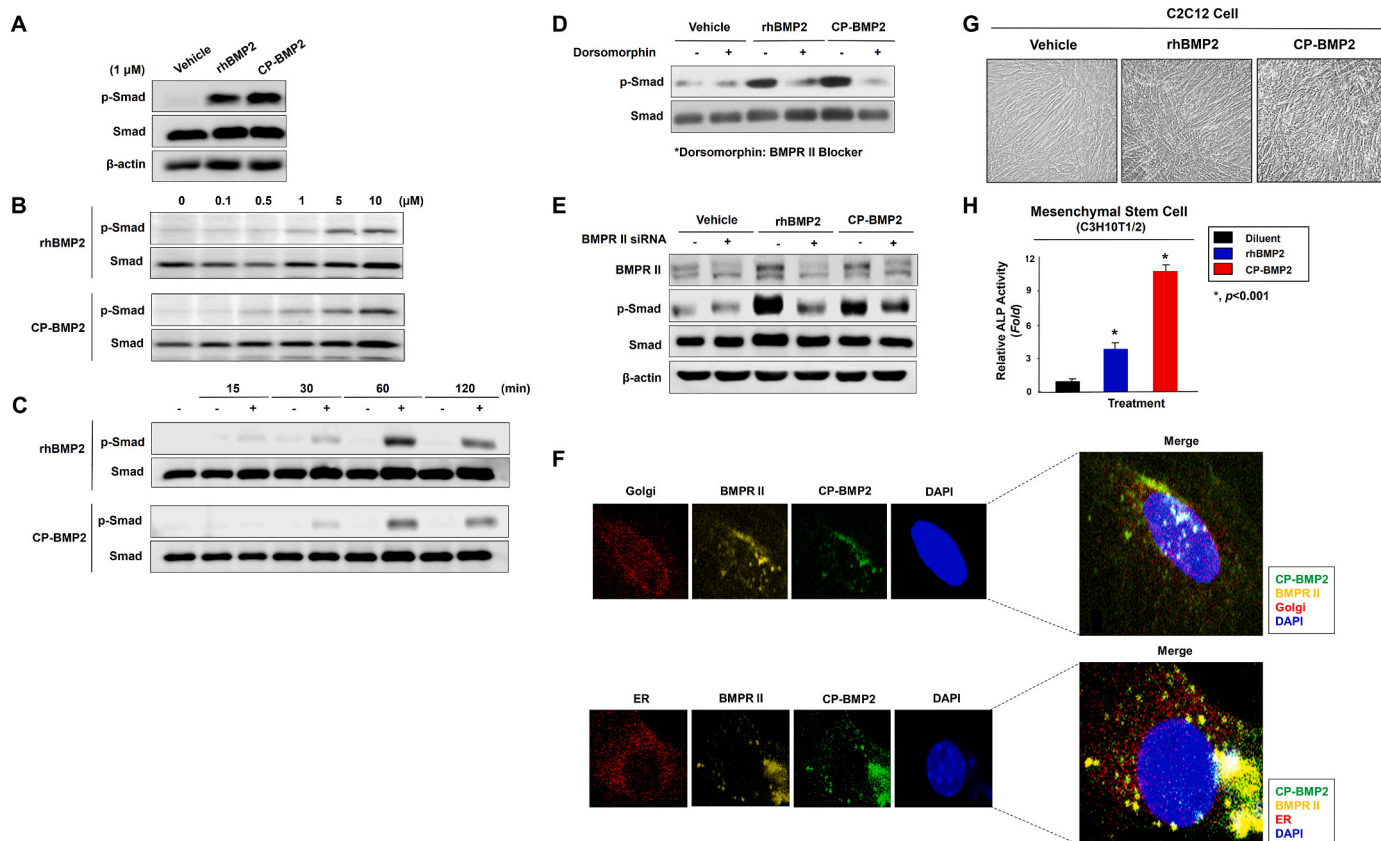


Fig. 2. CP-BMP2 activates the BMP2 signaling pathway through BMPR II binding. (A) Western blot analysis of *p*-Smad and Smad following treatment of rhBMP2 and CP-BMP2 (1 μ M) treatment. (B) Dose-dependent activation of *p*-Smad by rhBMP2 and CP-BMP2 (0–10 μ M) treatment. (C) Time-dependent activation of *p*-Smad by rhBMP2 and CP-BMP2 after 0, 15, 30, 60, and 120 min. (D) Treatment with the rhBMP2 antagonist dorsomorphin inhibited the ability of CP-BMP2 to increase *p*-Smad levels. (E) Depletion of BMPR II by treatment of its own siRNA decreased *p*-Smad activation by CP-BMP2. Cells were treated with vehicle, rhBMP2, or CP-BMP2 at identical concentrations for the same duration as described. (F) Representative confocal images of co-localization of CP-BMP2 (green) and BMPR II (yellow). (G) Morphological changes in C2C12 cells following CP-BMP2 treatment. (H) ALP activity in mesenchymal stem cells (C3H10T1/2) following CP-BMP2 treatment. (For interpretation of the references to color in this figure legend, the reader is referred to the Web version of this article.)

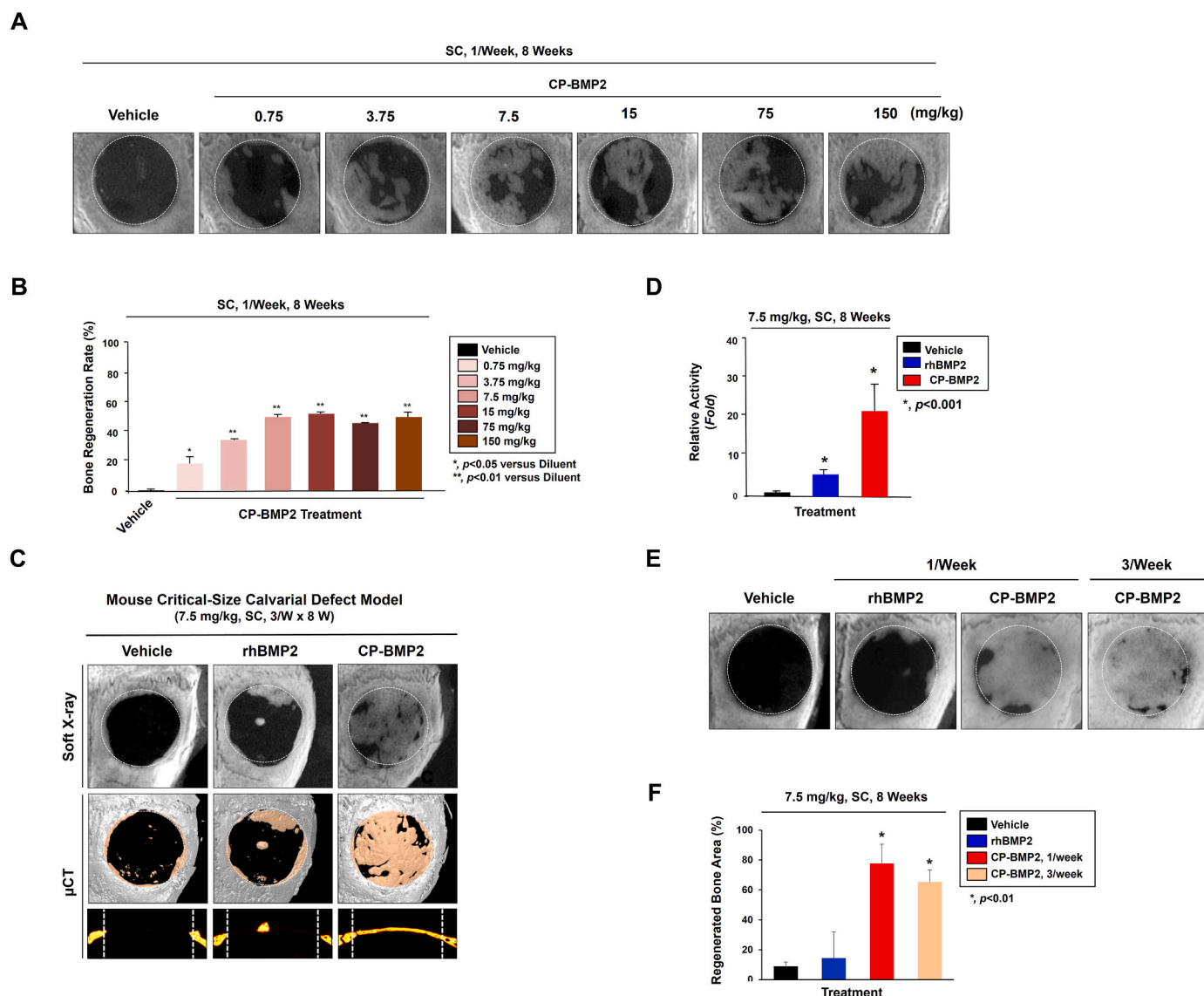


Fig. 3. CP-BMP2 enhances bone regeneration in a mouse critical-size calvarial defect model. (A) Soft X-ray acquired 8 weeks after repeated subcutaneous injections of CP-BMP2 at different doses from 0.75 to 150 mg/kg (1 times per week for 8 weeks). Vehicle was injected at an identical concentration and frequency. (B) Quantification of relative bone regeneration activity based on the surface area of new bone tissue covering the defect area when animals were treated with different dosages of CP-BMP2. (c and d) Soft X-ray images and μ CT images (C) and quantification (D) of the relative amount (area coverage, %) of regenerated bone according to the frequency (3 times per week) of treatment with 7.5 mg/kg CP-BMP2. (e and f) Soft X-ray images (E) and quantification of the relative amount (area coverage, %) (F) of regenerated bone when animals were treated with 7.5 mg/kg ~~once~~ 1 or 3 times per week for 8 weeks.

evaluated by counting pixels in the covered area of the calvarial defect using ImageJ software (National Institutes of Health, Bethesda, MD). Animals treated with CP-BMP2 without a scaffold showed more than 4-fold greater defect recovery, as measured by pixel area, compared to those treated with only rhBMP2 (Fig. 3D). CP-BMP2 treatment stimulates bone regeneration to a greater extent than rhBMP2 alone, which requires a scaffold. To find the optimal frequency for treatment, we conducted a study in which mice were SC injected with either vehicle, rhBMP2 or CP-BMP2 at a dose of 7.5 mg/kg, either once per week or three times per week for 8 weeks. The bone regeneration was evaluated, and we found that the mice receiving CP-BMP2 once per week or three times per week showed similar recovery levels of 78 % and 65 %, respectively (Fig. 3E and F). Based on these results, the optimal frequency, dose, and duration were determined to be 7.5 mg/kg with once per week for 8 weeks. The results indicate that treating calvarial defects with CP-BMP2 is more effective in terms of bone regeneration compared to treatment with rhBMP2 without a scaffold.

3.5. CP-BMP2 enhances bone repair in a rabbit bone defect model

After finding the ideal dose of CP-BMP2 for small animal models (mice), we evaluated its effect on bone healing in rabbits with critical-size calvarial defect. The rabbits received SC injections of either a placebo, rhBMP2, or CP-BMP2 at a dose of 7.5 mg/kg, three times per week, for 8 weeks without any scaffold support. To assess the bone regeneration, we used micro-CT imaging. Our results showed that both rhBMP2 and CP-BMP2 induced bone regeneration to a similar extent. However, the pattern of bone regeneration and degree of inflammation were noticeably different between the two groups (as shown in Fig. 4A). In particular, the defects in the rabbits treated with rhBMP2 recovered gradually from the edges, with some signs of inflammation, while the rabbits treated with CP-BMP2 recovered faster and steadily from the center of the defect. Additionally, the two groups exhibited distinct morphologies in histological sections of the calvaria defect samples taken at 8-week intervals. Furthermore, CP-BMP2 induced osteogenesis

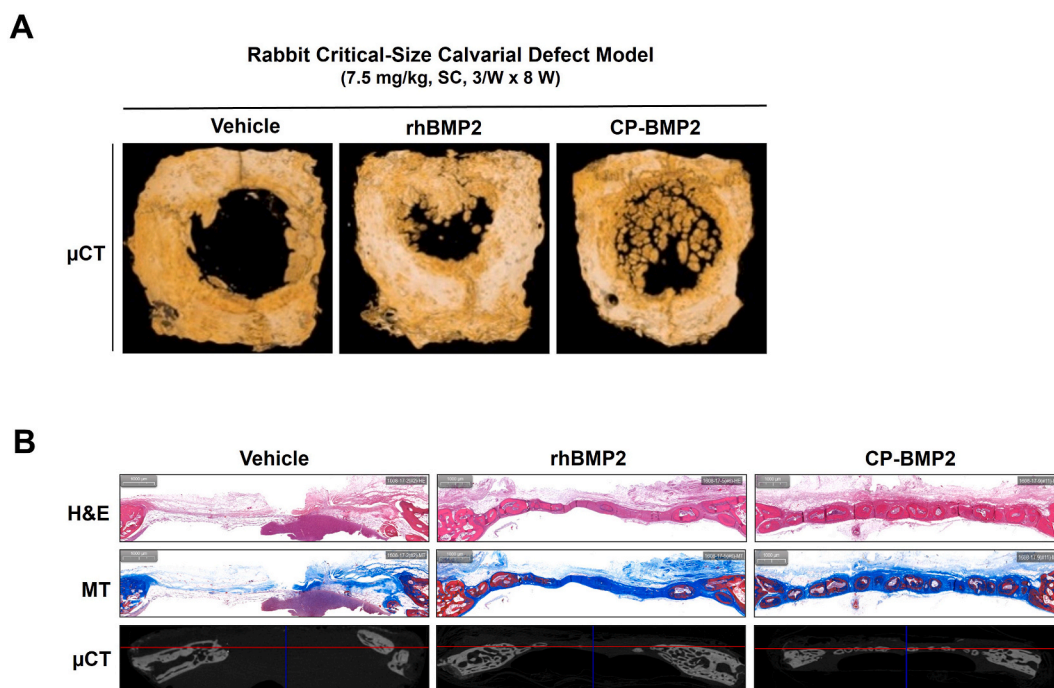


Fig. 4. CP-BMP2 enhances bone regeneration in a rabbit critical-size calvarial defect model. (A) μ CT images acquired 8 weeks after repeated subcutaneous injections of 7.5 mg/kg CP-BMP2 (3 times per week for 8 weeks). (B) Histological analysis of bone tissue cross-sections following CP-BMP2 treatment. For histological analysis, hematoxylin & eosin and Masson's trichrome staining was performed.

from the inside of the defect, while rhBMP2 did so from the edges (as shown in Fig. 4B). It is worth noting that the control group showed no signs of bone regeneration 8 weeks after treatment initiation. Our findings suggest that CP-BMP2 is more effective than rhBMP2 in both rodent and non-rodent models in the absence of scaffold support.

3.6. CP-BMP2 promotes bone regeneration in large animals without scaffold

To examine the effect of CP-BMP2 on bone regeneration in large animals, three-hole defects in the 3rd metatarsal bones of hind limbs were created in racehorses (Fig. 5A). One limb received three treatments (vehicle, rhBMP2, and CP-BMP2) without scaffolds (150 μ g/defect) once a week for 8 weeks, while the other limb received the same three treatments with scaffolds in a randomized manner. The assessment of bone fracture healing involved the use of Portable X-ray at various time points both before and after the operation. Radiographic data analysis using ImageJ yielded significant insights. Notably, CP-BMP2, when administered without a scaffold, demonstrated a superior bone regeneration rate of 33 % compared to rhBMP2 without a scaffold at the 9-week mark (the upper panel in Fig. 5B or the right panel in Fig. 5C). Conversely, when both rhBMP2 and CP-BMP2 were applied with scaffolds, they exhibited a comparable degree of bone regeneration (as illustrated in the lower panel of Fig. 5B or the left panel of Fig. 5C). The effectiveness of CP-BMP2 treatment without a scaffold was further supported by Micro-CT imaging, highlighting substantial morphological recovery (Fig. 5D). Quantitative analysis of the micro-CT images emphasized that CP-BMP2's ability to regenerate bone without a scaffold surpassed that of rhBMP2 by more than 85 % (Fig. 5E).

These results demonstrate that CP-BMP2 effectively promotes bone regeneration without a scaffold, showing a clear difference from rhBMP2. Our micro-CT results were confirmed histologically. Tissue samples from animals treated with rhBMP2 or CP-BMP2 showed clear evidence of osteoblast activation and woven bone formation (Fig. 5F). Additionally, a cement line was observed at the border of the compact bone, signifying the deposition of new bone material [41]. In particular,

animals treated with CP-BMP2 exhibited an increased fibroblast proliferation around the membrane. While rhBMP2 treatment showed higher levels of osteoblast activation and woven bone compared to the vehicle group, CP-BMP2 treatment showed a larger area of bone regeneration, covering most of the previously damaged area. This suggests that CP-BMP2 is more effective than rhBMP2 in promoting bone regeneration in large animals, particularly in the absence of a scaffold. In contrast, treatment with the vehicle or rhBMP2 resulted in the presence of macrophages, giant cells, and fibroblasts surrounding the scaffold, along with dead cells in the defect center.

4. Discussion

In this study, we developed CP-BMP2, an engineered form of BMP2, which showed superior cell permeability and increased bioavailability compared to rhBMP2 when administered in circulation. We assessed the therapeutic potential of CP-BMP2 for bone regeneration using three animal models (mouse, rabbit, and horse). Our findings highlight several advantages of CP-BMP2 over the current biologic, rhBMP2, which typically requires a scaffold for treating bone defects. Firstly, CP-BMP2 addresses stability issues observed in other cell-based agents, including rhBMP2, bone marrow mesenchymal stem cells, and adipose tissue-derived stem cells, when exposed to biofluids. This enhanced stability makes CP-BMP2 highly promising for preclinical and clinical trials. Secondly, CP-BMP2 can be conveniently administered through simple syringe-based injections, eliminating the need for painful surgeries, carrier scaffolds, or additional implants often associated with rhBMP2 treatment. Lastly, the unique properties of CP-BMP2 suggest that lower doses (e.g., 3.75–7.5 mg/kg) may be effective in clinical applications compared to rhBMP2. This dose reduction could offer significant benefits in terms of cost-effectiveness and reduced potential side effects. Thus, our study demonstrates that CP-BMP2 represents an innovative approach with significant potential as an osteogenic agent for bone regeneration.

The biological activity of BMP2 can be assessed through in vitro and in vivo methods. In vitro evaluation involves measuring the activation of

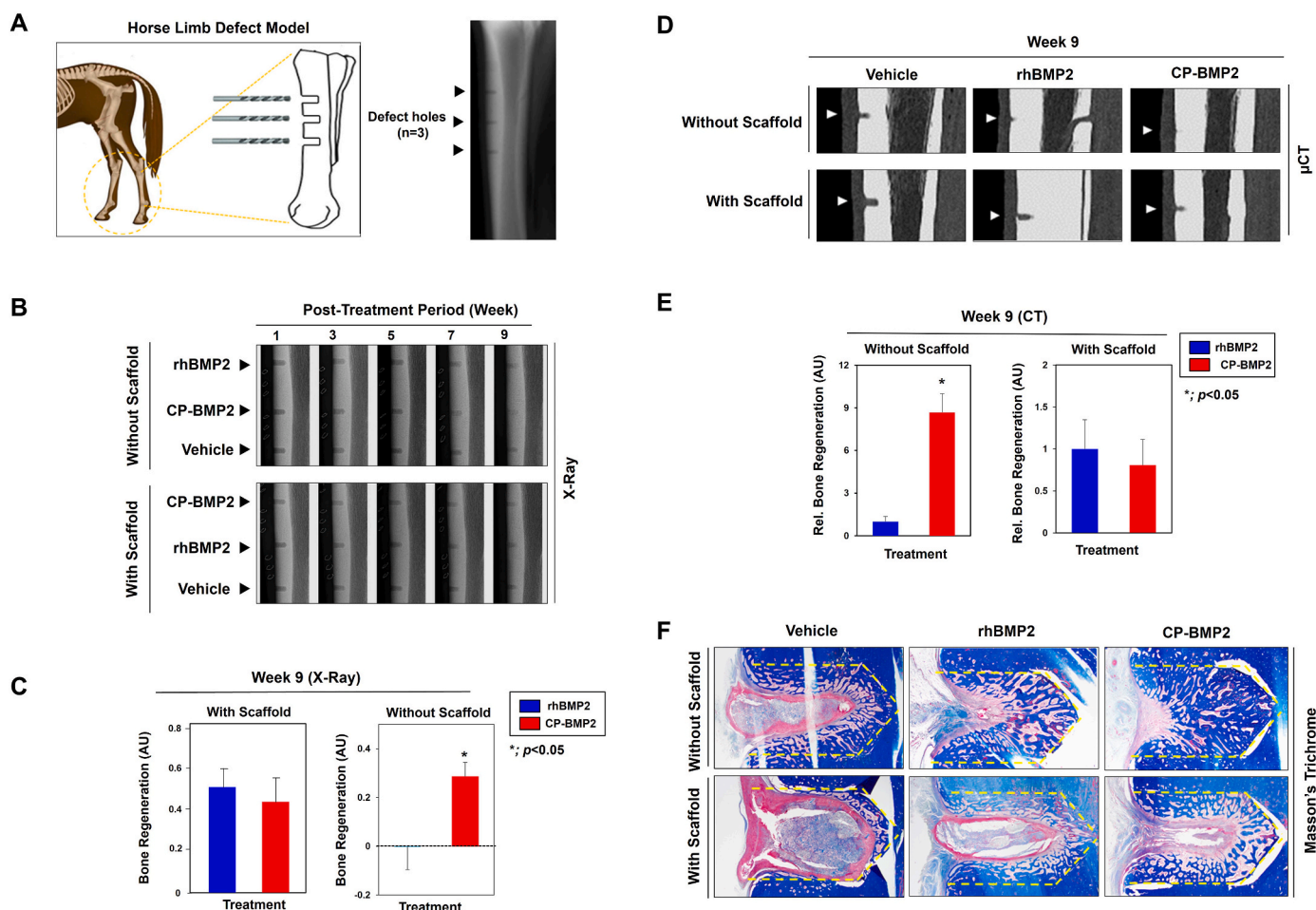


Fig. 5. CP-BMP2 without a collagen scaffold can enhance bone regeneration in a horse limb defect model. (A) Schematic diagram of the horse limb defect model and X-ray images showing 3 defect holes per hind limb. CP-BMP2 was administered with or without a collagen scaffold ($n = 6$). (B) X-ray images captured at several time points: 1, 3, 5, 7, and 9 weeks. (C) Quantification of bone regeneration based on X-ray images captured at week 9. (d and e) CT images (D) and quantification (E) of bone regeneration in the limb area at week 9. (F) Histological analysis of bone tissue cross-sections following CP-BMP2 treatment. For histological analysis, Masson's trichrome staining was performed. The yellow-dotted line indicates the original defect bone area. (For interpretation of the references to color in this figure legend, the reader is referred to the Web version of this article.)

the Smad signaling pathway and the transformation of myoblasts into osteoblasts using the C2C12 cell model [42]. Another approach is to observe the stimulation of alkaline phosphatase (ALP) activity, a marker of osteogenesis, through the BMP-2 signaling pathway [10]. In our study, we examined the effects of adding a specific CPP called aMTD442 to C2C12 cells. We found that the addition of aMTD442 enhanced the phosphorylation of R-Smads in a dose- and time-dependent manner. This was accompanied by a change in cell morphology towards an osteoblastic shape and an increase in ALP activity and in particular, CP-BMP2 can enter the cell directly by aMTD442 and directly bind to BMPR present in the Golgi apparatus and ER, so it can be seen that it tends to be independent of cell surface receptors (Fig. 2). These results suggest that the inclusion of aMTD442 does not impede the ability of rhBMP2 to promote bone regeneration and that CP-BMP2 functions identically to rhBMP2 in cells either directly or indirectly through BMPR II-independent Smad signaling. However, further investigation is required to understand how aMTD442 enhances the interaction between rhBMP2 and BMPR2 and strengthens the osteogenic signaling pathway. Additional research will shed light on the underlying mechanisms and provide a comprehensive understanding of the synergistic effects of aMTD442 and rhBMP2 in bone regeneration.

Exogenous administration of osteogenic proteins to promote tissue healing often leads to undesired tissue formation, immunogenicity, and necessitates invasive procedures, thus limiting its clinical utility [43].

The key to successful bone regeneration lies in maintaining a sufficient concentration of bone healing factors, such as BMP2, with prolonged activity specifically at the site of the bone defect. Ideally, protein-based biologics should be delivered intracellularly to achieve optimal plasma levels and target the precise area of the bone defect (Figs. 3 and 4). CP-BMP2, with its ability to facilitate direct transmission of rhBMP2 into cells, tissues, and body fluids, while also enabling longer retention at the bone defect site, offers a potential solution. This innovative approach may require lower doses and provide enhanced osteogenic differentiation effects by combining prolonged retention and improved delivery efficiency. Moreover, the hydrophobic nature of the aMTD platform employed for intracellular BMP2 delivery, demonstrated across model animals with varying body sizes, makes it a promising candidate for delivering other biologics, thereby expanding their therapeutic potential (Figs. 3–5). Further investigations are necessary to comprehensively understand the pharmacodynamics and mechanism of action underlying the effectiveness of CP-BMP2. Continued research in this area will shed light on the intricate workings of CP-BMP2 and advance our knowledge of its therapeutic applications.

The clinical application of protein-based biologics is confronted with several challenges, including poor solubility, rapid degradation, internalization, and fast clearance from circulation following administration. In response, the fields of regenerative medicine and drug delivery have developed various strategies to create stable recombinant proteins

capable of targeted delivery for promoting bone healing. These approaches often involve combining elements such as scaffolds, osteogenic proteins, stem cells, and genetic material to enhance osteogenesis and bone regeneration [44]. Comparative studies between these modified treatments and BMP2 alone have demonstrated a significant enhancement in the ability to heal bones and an extended presence of the therapeutic agent within bone defects across diverse animal models [44].

Our research indicates that CP-BMP2 has the potential to replace rhBMP2 treatment combined with a scaffold. This innovative approach effectively overcomes many inherent challenges associated with the clinical utilization of protein-based biologics. The presence of advanced macromolecular transduction domains (aMTDs) in CP-BMP2 likely contributes to its success by facilitating efficient protein transport across the plasma membrane, improving stability, and enhancing permeability [35]. Mechanistically, the short hydrophobic CPP sequences consisting of 12 amino acids enable proteins to directly cross the plasma membrane by insertion into the lipid bilayer, without requiring an energy source [35].

Studies have shown that the controlled or burst release of BMP2 enhances osteogenesis [45–48]. However, the rapid degradation of rhBMP2 after initial release presents a challenge. To address this, previous studies on horse bone regeneration using rhBMP2 have utilized carriers to retain the protein at the defect site [44,49,50]. These studies have indicated that a collagen scaffold may protect rhBMP2 from rapid clearance. Interestingly, in the absence of a 3D scaffold, CP-BMP2 was found to fill the gap in the equine bone defect model and showed accelerated bone regeneration compared to rhBMP2 (Fig. 5). Repeated administration of CP-BMP2 (3 injections) without a scaffold also significantly increased bone regeneration in the equine model (Fig. 5D and E). This suggests that CP-BMP2 is retained longer at the damaged site than rhBMP2, even without a scaffold or carrier. These findings highlight the difference between scaffold-supported rhBMP2 and aMTD-mediated rhBMP2 (CP-BMP2) in terms of sustainable efficacy for bone regeneration. CP-BMP2 has also the potential to shorten therapy duration for bone injury without causing complications.

5. Conclusion

CP-BMP2 demonstrates superiority over BMP2 based on three key factors: (1) Efficient Cell-to-Cell Transfer Mechanism: CP-BMP2 leverages aMTD's efficient cell-to-cell transfer mechanism, facilitating enhanced delivery across both outer and inner bone layers. This mechanism ensures the effective transportation of proteins to preosteocytes within damaged bones. (2) Direct Penetration to Preosteocytes and Osteocytes: In addition to the cell-to-cell transfer mechanism, CP-BMP2 exhibits the ability to reach preosteocytes and osteocytes through direct penetration. This dual approach activates both receptor-dependent and receptor-independent Smad signaling pathways. (3) Prolonged Therapeutic Effects: CP-BMP2 has the potential to remain in the body for an extended period, ensuring continuous therapeutic effects. This persistent presence activates p-Smad, inducing the expression of the bone formation biomarker ALP, ultimately promoting rapid osteogenesis. In conclusion, our findings strongly support the potential further development of CP-BMP2 as an osteogenic biobetter drug candidate. This innovative compound enhances local bone growth by sustaining the activation of the osteogenic signaling pathway in the affected bone-defect area.

Funding

This work was supported by a grant from the Small and Medium Business Administration (S2369334, Korea). The funders had no role in study design, data collection and analysis, the decision to publish, or manuscript preparation.

CRedit authorship contribution statement

Mingu Kang: Conceptualization, Data curation, Formal analysis, Investigation, Methodology, Project administration, Resources, Validation, Visualization, Writing – review & editing. **Seokwon Lee:** Data curation, Formal analysis, Investigation, Methodology, Resources, Validation, Visualization, Writing – review & editing. **Jong-pil Seo:** Conceptualization, Data curation, Formal analysis, Investigation, Methodology, Project administration, Resources, Validation, Visualization. **Eun-bee Lee:** Formal analysis, Investigation, Methodology, Validation, Visualization. **Daye Ahn:** Formal analysis, Investigation, Validation, Visualization. **Jisoo Shin:** Formal analysis, Investigation, Validation, Visualization. **Young-Ki Paik:** Conceptualization, Formal analysis, Methodology, Supervision, Validation, Writing – original draft, Writing – review & editing. **Daewoong Jo:** Conceptualization, Data curation, Formal analysis, Funding acquisition, Methodology, Project administration, Resources, Supervision, Validation, Writing – original draft, Writing – review & editing.

Declaration of competing interest

The authors declare that they have no known competing financial interests or personal relationships that could have appeared to influence the work reported in this paper.

Data availability

Data will be made available on request.

Acknowledgments

We extend our sincere appreciation to our staff scientists, Jaehyeon Kim, Youngjin Seo, Kiwoong Kwon, and Sungwon Cho. Their invaluable contributions, whether as project team leaders or teammates, have been marked by technical expertise and unwavering support throughout this study. We express deep gratitude for their dedicated efforts and significant contributions over the years. It is important to note that all animal handling and experimental procedures adhered to the guidelines set forth by the Institutional Review Board (IRB) of the Cellivity R&D Institute, Cellivity Therapeutics, Inc.

Appendix A. Supplementary data

Supplementary data to this article can be found online at <https://doi.org/10.1016/j.mtbio.2024.100983>.

References

- [1] T.O. Josephson, E.F. Morgan, Harnessing mechanical cues in the cellular microenvironment for bone regeneration, *Front. Physiol.* 14 (2023) 1232698, <https://doi.org/10.3389/fphys.2023.1232698>.
- [2] A. Arthur, S. Gronthos, Clinical application of bone marrow mesenchymal stem/Stromal cells to repair skeletal tissue, *Int. J. Mol. Sci.* 21 (24) (2020) 9759, <https://doi.org/10.3390/ijms21249759>.
- [3] B. Safari, S. Davaran, A. Aghanejad, Osteogenic potential of the growth factors and bioactive molecules in bone regeneration, *Int. J. Biol. Macromol.* 175 (2021) 544–557, <https://doi.org/10.1016/j.ijbiomac.2021.02.052>.
- [4] K. Hashimoto, T. Kaito, M. Furuya, S. Seno, D. Okuzaki, J. Kikuta, H. Tsukazaki, H. Matsuda, H. Yoshikawa, M. Ishii, In vivo dynamic analysis of BMP-2-induced ectopic bone formation, *Sci. Rep.* 10 (1) (2020) 4751, <https://doi.org/10.1038/s41598-020-61825-2>.
- [5] D. Halloran, H.W. Durbano, A. Nohe, Bone morphogenetic protein-2 in development and bone homeostasis, *J. Dev. Biol.* 8 (3) (2020) 19, <https://doi.org/10.3390/jdb8030019>.
- [6] R. Huntley, E. Jensen, R. Gopalakrishnan, K.C. Mansky, Bone morphogenetic proteins: their role in regulating osteoclast differentiation, *BoneKey Rep.* 10 (2019) 100207, <https://doi.org/10.1016/j.bonr.2019.100207>.
- [7] M. Wu, G. Chen, Y.P. Li, TGF- β and BMP signaling in osteoblast, skeletal development, and bone formation, homeostasis and disease, *Bone Res* 4 (2016) 16009, <https://doi.org/10.1038/boneres.2016.9>.

- [8] M.S. Rahman, N. Akhtar, H.M. Jamil, R.S. Banik, S.M. Asaduzzaman, TGF- β /BMP signaling and other molecular events: regulation of osteoblastogenesis and bone formation, *Bone Res* 3 (2015) 15005, <https://doi.org/10.1038/boneres.2015.5>.
- [9] J. McKie, S. Qureshi, J. Iatridis, N. Egorova, S. Cho, A. Hecht, Trends in bone morphogenetic protein usage since the U.S. Food and drug administration advisory in 2008: what happens to physician practices when the food and drug administration issues an advisory? *Global Spine J.* 4 (2) (2014) 71–76, <https://doi.org/10.1055/s-0033-1363515>.
- [10] G. Chen, C. Deng, Y.P. Li, TGF- β and BMP signaling in osteoblast differentiation and bone formation, *Int. J. Biol. Sci.* 8 (2) (2012) 272–288, <https://doi.org/10.7150/ijbs.2929>.
- [11] R.N. Wang, J. Green, Z. Wang, Y. Deng, M. Qiao, M. Peabody, Q. Zhang, J. Ye, Z. Yan, S. Denduluri, O. Idowu, M. Li, C. Shen, A. Hu, R.C. Haydon, R. Kang, J. Mok, M.J. Lee, H.L. Luu, L.L. Shi, Bone Morphogenetic Protein (BMP) signaling in development and human diseases, *Genes Dis* 1 (1) (2014) 87–105, <https://doi.org/10.1016/j.gendis.2014.07.005>.
- [12] B. Gamez, E. Rodriguez-Carballo, F. Ventura, BMP signaling in telencephalic neural cell specification and maturation, *Front. Cell. Neurosci.* 7 (2013) 87, <https://doi.org/10.3389/fncel.2013.00087>.
- [13] K. Yang, X.D. Tang, W. Guo, X.L. Xu, T.T. Ren, C.M. Ren, S.D. Wang, X. Bao, F. Zhang, K.K. Sun, BMP2-pSMAD1/5 signaling pathway regulates RUNX2 expression and impacts the progression of dedifferentiated chondrosarcoma, *Am. J. Cancer Res.* 6 (6) (2016) 1302–1316, PMID: PMC4937734.
- [14] Y. Niu, Z. Wang, Y. Shi, L. Dong, C. Wang, Modulating macrophage activities to promote endogenous bone regeneration: biological mechanisms and engineering approaches, *Bioact. Mater.* 6 (1) (2020) 244–261, <https://doi.org/10.1016/j.bioactmat.2020.08.012>.
- [15] J. Jann, O. Drevelle, M.A. Lauzon, N. Fauchoux, Adhesion, intracellular signalling and osteogenic differentiation of mesenchymal progenitor cells and preosteoblasts on poly(epsilon)caprolactone films functionalized by peptides derived from fibronectin and/or BMP-9, *Mater. Sci. Eng., C* 114 (2020) 111088, <https://doi.org/10.1016/j.msec.2020.111088>.
- [16] B. Bragdon, O. Moseychuk, S. Saldanha, D. King, J. Julian, A. Nohe, Bone morphogenetic proteins: a critical review, *Cell. Signal.* 23 (4) (2011) 609–620, <https://doi.org/10.1016/j.cellsig.2010.10.003>.
- [17] L. Bai, H.M. Chang, L. Zhang, Y.M. Zhu, P.C. Leung, BMP2 increases the production of BDNF through the upregulation of proBDNF and furin expression in human granulosa-lutein cells, *Faseb. J.* 34 (12) (2020) 16129–16143, <https://doi.org/10.1096/fj.202000940R>.
- [18] B. Huang, Y. Yuan, T. Li, S. Ding, W. Zhang, Y. Gu, C. Liu, Facilitated receptor-recognition and enhanced bioactivity of bone morphogenetic protein-2 on magnesium-substituted hydroxyapatite surface, *Sci. Rep.* 6 (2016) 24323, <https://doi.org/10.1038/srep24323>.
- [19] Z. Amso, J. Cornish, M.A. Brimble, Short anabolic peptides for bone growth, *Med. Res. Rev.* 36 (4) (2016) 579–640, <https://doi.org/10.1002/med.21388>.
- [20] B. Huang, Y. Yuan, T. Li, S. Ding, W. Zhang, Y. Gu, C. Liu, Facilitated receptor-recognition and enhanced bioactivity of bone morphogenetic protein-2 on magnesium-substituted hydroxyapatite surface, *Sci. Rep.* 6 (2016) 24323, <https://doi.org/10.1038/srep24323>.
- [21] I.E. Bialy, W. Jiskoot, M.R. Nejadnik, Formulation, delivery and stability of bone morphogenetic proteins for effective bone regeneration, *Pharm. Res. (N. Y.)* 34 (6) (2017) 1152–1170, <https://doi.org/10.1007/s11095-017-2147-x>.
- [22] A.C. Carreira, F.H. Lojudice, E. Halcsik, R.D. Navarro, M.C. Sogayar, J. M. Granjeiro, Bone morphogenetic proteins: facts, challenges, and future perspectives, *J. Dent. Res.* 93 (4) (2014) 335–345, <https://doi.org/10.1177/0022034513518561>.
- [23] G. Hulsart-Billstrom, P.K. Yuen, R. Marsell, J. Hilborn, S. Larsson, D. Ossipov, Bisphosphonate-linked hyaluronic acid hydrogel sequesters and enzymatically releases active bone morphogenetic protein-2 for induction of osteogenic differentiation, *Biomacromolecules* 14 (9) (2013) 3055–3063, <https://doi.org/10.1021/bm400639e>.
- [24] B.J. Zhang, Z.W. Han, K. Duan, Y.D. Mu, J. Weng, Multilayered pore-closed PLGA microsphere delivering OGP and BMP-2 in sequential release patterns for the facilitation of BMSCs osteogenic differentiation, *J. Biomed. Mater. Res.* 106 (1) (2018) 95–105, <https://doi.org/10.1002/jbm.a.36210>.
- [25] X. Lin, K. de Groot, D. Wang, Q. Hu, D. Wismeijer, Y. Liu, A review paper on biomimetic calcium phosphate coatings, *Open Biomed. Eng. J.* 9 (2015) 56–64, <https://doi.org/10.2174/18741207101509010056>.
- [26] M. Maisani, K.R. Sindhu, M. Fenelon, R. Siadous, S. Rey, D. Mantovani, O. Chassande, Prolonged delivery of BMP-2 by a non-polymer hydrogel for bone defect regeneration, *Drug Deliv Transl Res* 8 (1) (2018) 178–190, <https://doi.org/10.1007/s13346-017-0451-y>.
- [27] X. Xu, J. Song, Segmental long bone regeneration guided by degradable synthetic polymeric scaffolds, *Biomater Transl* 1 (1) (2020) 33–45, <https://doi.org/10.3877/cma.j.issn.2096-112X.2020.01.004>.
- [28] X. Chen, B. Tan, Z. Bao, S. Wang, R. Tang, Z. Wang, G. Chen, S. Chen, W.W. Lu, D. Yang, S. Peng, Enhanced bone regeneration via spatiotemporal and controlled delivery of a genetically engineered BMP-2 in a composite Hydrogel, *Biomaterials* 277 (2021) 121117, <https://doi.org/10.1016/j.biomaterials.2021.121117>.
- [29] J.D. Boerckel, Y.M. Kolambkar, K.M. Dupont, B.A. Uhrig, E.A. Phelps, H.Y. Stevens, A.J. Garcia, R.E. Guldberg, Effects of protein dose and delivery system on BMP-mediated bone regeneration, *Biomaterials* 32 (22) (2011) 5241–5251, <https://doi.org/10.1016/j.biomaterials.2011.03.063>.
- [30] H.J. Lee, A.N. Koo, S.W. Lee, M.H. Lee, S.C. Lee, Catechol-functionalized adhesive polymer nanoparticles for controlled local release of bone morphogenetic protein-2 from titanium surface, *J. Contr. Release* 170 (2) (2013) 198–208, <https://doi.org/10.1016/j.jconrel.2013.05.017>.
- [31] K.W. Lo, B.D. Ulery, K.M. Ashe, C.T. Laurencin, Studies of bone morphogenetic protein-based surgical repair, *Adv. Drug Deliv. Rev.* 64 (12) (2012) 1277–1291, <https://doi.org/10.1016/j.addr.2012.03.014>.
- [32] Y.M. Kolambkar, J.D. Boerckel, K.M. Dupont, M. Bajin, N. Huebsch, D.J. Mooney, D.W. Huttmacher, R.E. Guldberg, Spatiotemporal delivery of bone morphogenetic protein enhances functional repair of segmental bone defects, *Bone* 49 (3) (2011) 485–492, <https://doi.org/10.1016/j.bone.2011.05.010>.
- [33] N.H. Kim, Y.H. Cha, H.S. Kim, S.E. Lee, J.K. Huh, J.K. Kim, J.M. Kim, J.K. Ryu, H. J. Kim, Y. Lee, S.Y. Lee, I. Noh, X.Y. Li, S.J. Weiss, T.A. Jahng, J.I. Yook, A platform technique for growth factor delivery with novel mode of action, *Biomaterials* 35 (37) (2014) 9888–9896, <https://doi.org/10.1016/j.biomaterials.2014.08.005>.
- [34] C.H. Jeong, S.Y. Lim, J.E. Um, H.W. Lim, K.H. Hwang, K.M. Park, J.S. Yun, D. H. Kim, J.K. Huh, H.S. Kim, J.I. Yook, N.H. Kim, Y.H. Kwak, Micellized protein transduction domain-bone morphogenetic protein-2 accelerates bone healing in a rat tibial distraction osteogenesis model, *Acta Biomater.* 170 (2023) 360–375, <https://doi.org/10.1016/j.actbio.2023.08.031>.
- [35] E. Chung, Y. Choi, J. Park, W. Nah, J. Park, Y. Jung, J. Lee, H. Lee, S. Park, S. Hwang, S. Kim, J. Lee, D. Min, J. Jo, S. Kang, M. Jung, P.H. Lee, H.E. Ruley, D. Jo, Intracellular delivery of Parkin rescues neurons from accumulation of damaged mitochondria and pathological alpha-synuclein, *Sci. Adv.* 6 (18) (2020), <https://doi.org/10.1126/sciadv.aba1193> eaba1193.
- [36] D. Jo, D. Liu, S. Yao, R.D. Collins, J. Hawiger, Intracellular protein therapy with SOCS3 inhibits inflammation and apoptosis, *Nat. Med.* 11 (8) (2005) 892–898, <https://doi.org/10.1038/nm1269>.
- [37] H. Kobayashi, T. Yoshida, M. Inouye, Significant enhanced expression and solubility of human proteins in *Escherichia coli* by fusion with protein S from *Myxococcus xanthus*, *Appl. Environ. Microbiol.* 75 (16) (2009) 5356–5362, <https://doi.org/10.1128/AEM.00691-09>.
- [38] T. Hirschhorn, M. Levi-Hofman, O. Danziger, N.I. Smorodinsky, M. Ehrlich, Differential molecular regulation of processing and membrane expression of Type-I BMP receptors: implications for signaling, *Cell. Mol. Life Sci.* 74 (14) (2017) 2645–2662, <https://doi.org/10.1007/s00018-017-2488-y>.
- [39] G.M. Cooper, M.P. Mooney, A.K. Gosain, P.G. Campbell, J.E. Losee, J. Huard, Testing the critical size in calvarial bone defects: revisiting the concept of a critical-size defect, *Plast. Reconstr. Surg.* 125 (6) (2010) 1685–1692, <https://doi.org/10.1097/PRS.0b013e3181cb63a3>.
- [40] Y. Zhang, L. Wang, F. Deng, H. Qiu, X. Wu, Determination of a critical size calvarial defect in senile osteoporotic mice model based on in vivo micro-computed tomography and histological evaluation, *Arch. Gerontol. Geriatr.* 61 (1) (2015) 44–55, <https://doi.org/10.1016/j.archger.2015.01.019>.
- [41] G. Luo, Y. Huang, F. Gu, rhBMP-2-loaded calcium phosphate cements combined with allogenic bone marrow mesenchymal stem cells for bone formation, *Biomed. Pharmacother.* 92 (2017) 536–543, <https://doi.org/10.1016/j.biopha.2017.05.083>.
- [42] S. Kokabu, T. Katagiri, T. Yoda, V. Rosen, Role of Smad phosphatases in BMP-Smad signaling axis-induced osteoblast differentiation, *J. Oral Biosci.* 54 (2) (2012) 73–78, <https://doi.org/10.1016/j.job.2012.02.003>.
- [43] A.W. James, G. LaChaud, J. Shen, G. Asatrian, V. Nguyen, X. Zhang, K. Ting, C. Soo, A review of the clinical side effects of bone morphogenetic protein-2, *Tissue Eng., Part B* 22 (4) (2016) 284–297, <https://doi.org/10.1089/ten.TEB.2015.0357>.
- [44] T. Xu, L. Sheng, L. He, J. Weng, K. Duan, Enhanced osteogenesis of hydroxyapatite scaffolds by coating with BMP-2-loaded short polylactide nanofiber: a new drug loading method for porous scaffolds, *Regen Biomater* 7 (1) (2020) 91–98, <https://doi.org/10.1093/rb/rbz040>.
- [45] F.Y. Teng, I.C. Tai, M.L. Ho, J.W. Wang, L.W. Weng, Y.J. Wang, M.W. Wang, C. T. Tseng, Controlled release of BMP-2 from titanium with electrodepositing modification enhancing critical size bone formation, *Mater. Sci. Eng., C* 105 (2019) 109879, <https://doi.org/10.1016/j.msec.2019.109879>.
- [46] T. Hu, M. Naidu, Z. Yang, W.M. Lam, R.A. Kumarsing, X. Ren, F. Ng, M. Wang, L. Liu, K.C. Tan, K.T. Kwok, S.B. Goodman, J.C. Goh, H.K. Wong, Bone regeneration by controlled release of bone morphogenetic protein-2: a rabbit spinal fusion chamber molecular study, *Tissue Eng.* 25 (19–20) (2019) 1356–1368, <https://doi.org/10.1089/ten.TEA.2018.0281>.
- [47] N. Deng, J. Sun, Y. Li, L. Chen, C. Chen, Y. Wu, Z. Wang, L. Li, Experimental study of rhBMP-2 chitosan nano-sustained release carrier-loaded PLGA/nHA scaffolds to construct mandibular tissue-engineered bone, *Arch. Oral Biol.* 102 (2019) 16–25, <https://doi.org/10.1016/j.archoralbio.2019.03.023>.
- [48] M.T. Howard, S. Wang, A.G. Berger, J.R. Martin, S. Jalili-Firoozinezhad, R. F. Padera, P.T. Hammond, Sustained release of BMP-2 using self-assembled layer-by-layer film-coated implants enhances bone regeneration over burst release, *Biomaterials* 288 (2022) 121721, <https://doi.org/10.1016/j.biomaterials.2022.121721>.
- [49] Y. Qiu, X. Xu, W. Guo, Y. Zhao, J. Su, J. Chen, Mesoporous hydroxyapatite nanoparticles mediate the release and bioactivity of BMP-2 for enhanced bone regeneration, *ACS Biomater. Sci. Eng.* 6 (4) (2020) 2323–2335, <https://doi.org/10.1021/acsbomaterials.9b01954>.
- [50] Q. Gan, H. Pan, W. Zhang, Y. Yuan, J. Qian, C. Liu, Fabrication and evaluation of a BMP-2/dexamethasone co-loaded gelatin sponge scaffold for rapid bone regeneration, *Regen Biomater* 16 (2022) 9, <https://doi.org/10.1093/rb/rbac008>, rbac008.